Morin-type spin-reorientation transition below the Néel transition in the monoclinic compositions of $(1-x)BiFeO_3$-$xPbTiO_3$ ($x = 0.25$ and 0.27): A combined dc magnetization and x-ray and neutron powder diffraction study

Shuvrajyoti Bhattacharjee,[1] Anatoliy Senyshyn,[2] Hartmut Fuess,[3] and Dhananjai Pandey[1,*]

[1]*School of Materials Science and Technology, Indian Institute of Technology (Banaras Hindu University), Varanasi-221005, India*

[2]*Forschungsneutronenquelle Heinz Maier-Leibnitz (FRM II), Technische Universitaet München, Lichtenbergestrasse 1, D-85747 Garching b. München, Germany*

[3]*Darmstadt University of Technology, Institute of Materials Science, Structure Research, Petersenstrasse, 23, D-64287 Darmstadt, Germany*

(Received 12 May 2012; revised manuscript received 30 November 2012; published 14 February 2013)

The dc magnetization $M(T)$ studies on monoclinic compositions of $(1-x)BiFeO_3$-$xPbTiO_3$ (BF-xPT), $x = 0.25$ and 0.27, reveal another anomaly at spin-reorientation phase transition (T_{OPT}) below the Néel transition temperature (T_N). From a Rietveld refinement of the magnetic structure using neutron powder diffraction data, it is shown that the anomaly at T_{OPT} is due to a spin-reorientation transition from a long-range magnetically ordered phase ($\boldsymbol{G}_y$, $\boldsymbol{F}_{xz}$) stable at $T_{OPT} < T < T_N$ to another long-range ordered phase ($\boldsymbol{G}_{xz}$, $\boldsymbol{F}_y$) stable below T_{OPT}, wherein the ferromagnetic component of the noncollinear magnetic structure undergoes a spin flop. The spin-reorientation transition is not linked with any structural phase transition as confirmed by x-ray diffraction studies. Further, this transition is not accompanied with any magnetoelastic coupling. Unlike the Néel transition, the spin-reorientation transition is purely of magnetic origin. The spin-reorientation transition in BF-xPT is similar to the Morin transition in hematite and differs from the spin-reorientation transition in orthoferrites that is driven by the coupling of two magnetic sublattices.

DOI: 10.1103/PhysRevB.87.054417 PACS number(s): 75.85.+t, 75.25.−j, 75.50.Ee

I. INTRODUCTION

Several antiferromagnetic insulators are known to exhibit a change in the easy axis of magnetization from one crystallographic direction to another leading to a change in the spin orientation as a function of temperature,[1–5] photoexcitation,[6] and interparticle interactions,[7] In recent years, spin-reorientation phase transition in antiferromagnetic insulators has attracted considerable attention due to the observation of ultrafast spin rotation times having potential technological applications.[8] Among the antiferromagnetic insulators, hematite[1] and orthoferrites[2–5] have been investigated extensively for spin-reorientation transition. In hematite (α-Fe_2O_3), the magnetic moments are parallel within the basal plane, while they are antiferromagnetically coupled with the moments in the neighboring planes below the Néel temperature ($T_N \sim 955$ K).[1] But below the spin-reorientation phase transition temperature $T_{OPT} \sim 263$ K, the moments rotate by 90° such that the spins in the basal plane are now aligned parallel to the c axis without affecting the antiferromagnetic coupling between the neighboring planes.[1] In orthoferrites ($ReFeO_3$ with Re = Er, Dy, Yr, Sc, Nd, etc.), upon cooling below the Néel temperature (T_N), the iron sublattice initially orders into the symmetry configuration as per the irreducible representation (IR) Γ_4 ($\boldsymbol{G}_x$, $\boldsymbol{F}_z$) (in Bertaut's notation[9]) such that the components of the ordered spins are antiferromagnetically coupled (G type) in the x direction and ferrromagnetically in the z direction of the unit cell of the orthorhombic structure in the *Pbnm* space group.[2] This phase undergoes two second-order spin-reorientation transitions, which can be expressed as $\Gamma_4(\boldsymbol{G}_x,\boldsymbol{F}_z)$ to $\Gamma_{24}(\boldsymbol{G}_{xz},\boldsymbol{F}_{xz})$ and $\Gamma_{24}(\boldsymbol{G}_{xz},\boldsymbol{F}_{xz})$ to $\Gamma_2(\boldsymbol{G}_z,\boldsymbol{F}_x)$ at temperatures T_1 and T_2, respectively. In the tilted Γ_{24} ($\boldsymbol{G}_{xz}$, $\boldsymbol{F}_{xz}$) phase, the ferromagnetic component F rotates in the ac plane continuously in the temperature interval (T_1,T_2) until it becomes parallel to the a axis ($\boldsymbol{F}_x$) at T_2. Thus, the spin-reorientation transition in orthoferrites is a continuous rotation of vector $\boldsymbol{F}$ with temperature from the c axis ($\boldsymbol{F}_z$) above T_1 toward the a axis ($\boldsymbol{F}_x$), such that $\boldsymbol{F}$ remains in the ac plane ($\boldsymbol{F}_{xz}$) during rotation in the temperature interval (T_1, T_2). The spin-reorientation transition in orthoferrites is supposed to be driven by the interaction between the Re and Fe magnetic sublattices.[2–4] Further, in both hematite and orthoferrites, there is no evidence of any structural change accompanying the spin-reorientation transition.[1,4]

The multiferroic compound $BiFeO_3$, like rare-earth orthoferrites ($ReFeO_3$), also possesses a tilted octahedral perovskite structure but with a tilt system ($a^-a^-a^-$ in Glazer's notation[10]) that is different from that of orthoferrites ($a^-a^-c^+$), leading to a change of space group from *Pbnm* for orthoferrites to *R*3*c* for $BiFeO_3$.[11] Spin-reorientation transitions have been reported in $BiFeO_3$ also, both above[12] and below[13] room temperature, using Raman scattering, magnetization, and ac susceptibility measurements. However, the existence of such reorientation transitions in $BiFeO_3$ has been questioned recently on the basis of magnetization and neutron scattering studies on single crystals that did not reveal such transitions.[14] In this paper, we present unambiguous evidence for spin-reorientation transition in a solid solution of $BiFeO_3$ with $PbTiO_3$ using magnetization and neutron scattering studies. As a result of $PbTiO_3$ substitution, the space group of the nuclear structure of $BiFeO_3$ changes from *R*3*c* to *Cc*.[15,16] This monoclinic structure in the solid solution system $(1-x)$BF-xPT (BF-xPT) is stable for $x \leqslant 0.27$ and undergoes a morphotropic phase transition to a tetragonal phase in the *P*4*mm* space group symmetry for $x \geqslant 0.31$ through a narrow composition range ($0.27 < x < 0.31$) over which the two phases coexist.[16,17] Our results show that the spin-reorientation transition is restricted only to the monoclinic compositions of BF-xPT. High-temperature

x-ray diffraction (XRD) measurements across the reorientation transition do not reveal any change of crystal structure and magnetoelastic coupling, confirming pure magnetic origin of this transition. The spin reorientation in BF-xPT is shown to be like Morin transition in hematite and differs from the spin reorientation in orthoferrites that is driven by the coupling of two magnetic sublattices.

II. EXPERIMENT

Two solid solution compositions of $(1-x)BiFeO_3$-$xPbTiO_3$ with $x = 0.25$ and 0.27 were prepared by solid-state reaction route, details of which have been reported previously.[17] Powder XRD measurements at room temperature and high temperatures were carried out using an 18-kW Cu-rotating anode-based Rigaku (Tokyo, Japan) powder diffractometer operating in Bragg-Brentano geometry and fitted with a crystal monochromator in the diffraction beam and also with a high-temperature attachment. The high-temperature XRD data were collected in the temperature range of 300 to 873 K and the 2θ range of 15–120° at a step of 0.02°. Powder neutron diffraction data at room and high temperatures for BF-0.25PT was collected using the high-resolution powder diffractometer SPODI at FRM-II, Germany.[18] The wavelength of the incident neutron beam was 1.548 Å. Rietveld refinement was carried out using Fullprof package and BasIrreps in the same package.[19] The temperature-dependent magnetization measurements in the temperature range 80 to 600 K at a magnetic field of 2500 Oe were carried out using a vibrating sample magnetometer (VSM-7305, Lakeshore) at a heating rate of 5 K/min.

III. RESULTS AND DISCUSSION

$BiFeO_3$ in bulk form has a rhombohedrally distorted perovskite structure with the $R3c$ space group symmetry. In this structure, two adjacent oxygen octahedra (FeO_6 unit) along the trigonal [111] direction are rotated in the opposite way, while Bi^{3+} and Fe^{3+} cations are displaced from their centrosymmetric positions. The $R3c$ structure is obtained from the cubic $Pm3m$ structure by freezing one of the zone center ($\boldsymbol{k} = 0,0,0$) modes (Γ_4^-) and an R-point ($\boldsymbol{k} = \frac{1}{2}\frac{1}{2}\frac{1}{2}$) mode ($R_4^+$). The rhombohedral phase of $BiFeO_3$ changes to monoclinic in thin films under stress.[20] We have recently shown that the bulk symmetry of $BiFeO_3$ also reduces from rhombohedral $R3c$ space group to the monoclinic Cc space group with the substitution of Pb^{2+} and Ti^{4+} for Bi^{3+} and Fe^{3+}cations, respectively.[15,16] In the pure BF, the ferroelectric polarization $\boldsymbol{P}$ is along [111] trigonal axis, but in the monoclinic phase the polarization vector $\boldsymbol{P}$ is free to rotate in the ac (or xz) plane. On the other hand, the room-temperature magnetic structure of the monoclinic Cc phase of BF-xPT corresponds to a noncollinear G-type antiferromagnet[21] in which the moments are antiferromagnetically coupled in the xz plane but ferromagnetically in the y direction ($\boldsymbol{G}_{xz}$, $\boldsymbol{F}_y$ in Bertaut notation[9]). The symmetry of the magnetic structure is such that the antiferromagnetic vector $\boldsymbol{G}_{xz}$ can rotate in the xz plane just like the polarization vector $\boldsymbol{P}$.

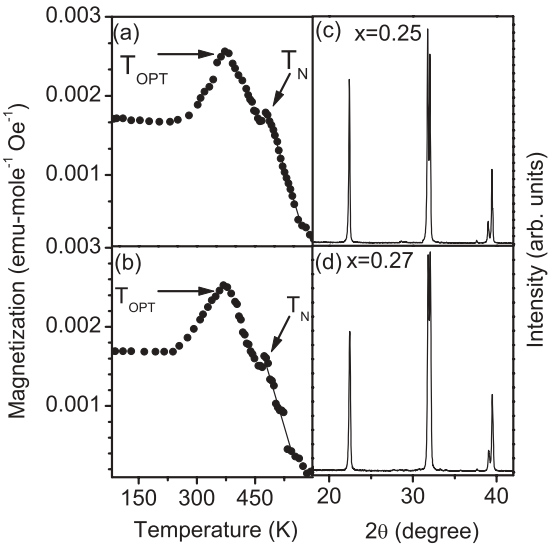

FIG. 1. Temperature dependence of dc magnetization (M) of BF-xPT for (a) $x = 0.25$ and (b) $x = 0.27$ showing two transitions at T_N and T_{OPT}. The room-temperature powder XRD profiles of BF-xPT with (c) $x = 0.25$, and (d) $x = 0.27$ in the 2θ range 20 to 42° showing monophasic nature of samples.

A. Evidence for an anomaly in $M(T)$ below the Néel temperature

Noncollinear antiferromagnetic ordering develops below the Néel temperature for the monoclinic compositions of BF-xPT.[21] A continuous rotation of the antiferromagnetic vector $\boldsymbol{G}$ may be observed in the monoclinic compositions below T_N, similar to the case of orthoferrites, if the xz symmetry plane coincides with the easy plane. Magnetization measurements in the presence of a moderate field (2500 Oe) were carried out in the temperature range from 80 to 600 K to capture any signature of the spin-reorientation transition in the monoclinic compositions of BF-xPT. The results of dc magnetization measurements $M(T)$ are shown in Figs. 1(a) and 1(b) for two monoclinic compositions with $x = 0.25$ and 0.27. The $M(T)$ plot shows two distinct anomalies. $BiFeO_3$ shows onset of long-range magnetic ordering below $T_N \sim 625$ K[22] with one anomaly in $M(T)$. With the doping of nonmagnetic $PbTiO_3$, the magnetic ordering temperature goes down and T_N changes to ~483 K for $x = 0.25$ and 473 K for $x = 0.27$,[21,23] as shown in Figs. 1(a) and 1(b). However, below T_N, another anomaly, which is quite broad, occurs at 370 and 367 K for $x = 0.25$ and $x = 0.27$, respectively. As will be explained in a subsequent section, the broad anomaly in $M(T)$ is due to a spin-reorientation phase transition (OPT), and we shall use the symbol T_{OPT} for distinguishing this transition temperature from the Néel transition temperature T_N henceforth.

B. Possible role of a coexisting phase

A broad anomaly at ~373 K, similar to that shown in Fig. 1 for 0.27, was also earlier reported by Zhu *et al.* [23] who attributed it to the paramagnetic to antiferromagnetic phase transition of a coexisting orthorhombic phase with a different T_N. However, the broad anomaly observed in $M(T)$ below T_N in our samples cannot be linked with some coexisting crystallographic phase, since both compositions ($x = 0.25$ and

0.27) are monophasic, as can be seen from Figs. 1(c) and 1(d), which depict the x-ray powder diffraction patterns in the 2θ range from 17 to 43° at room temperature for $x = 0.25$ and 0.27, respectively. Rietveld analysis of these data shows that the structure is not rhombohedral in the $R3c$ space group but is monoclinic in the Cc space group.[15,16] The diffraction pattern that was attributed to an orthorhombic phase by Zhu *et al.*[23] is now known to be due to the coexistence of tetragonal and monoclinic phases.[16]

In chemically homogeneous and strain-free samples of BF-xPT, it is now well established that the monoclinic and tetragonal phases are stable for $x \leqslant 0.27$ and $x \geqslant 0.31$, respectively,[16] with no evidence for any orthorhombic phase proposed by Zhu *et al.*,[23] whereas the two phases coexist in the MPB region $0.27 < x < 0.31$. However, it is also known that in stressed samples, such as those obtained after crushing the sintered pellets, the single-phase monoclinic compositions with $x \leqslant 0.27$ may become a two-phase mixture containing both tetragonal and monoclinic phases, as a result of a stress-induced monoclinic to tetragonal phase transition.[24] The XRD samples used by Zhu *et al.*[23] for $x \leqslant 0.27$ indeed show the coexistence of the tetragonal and monoclinic phases, possibly due to such a stress-induced transition. The question arises as to whether the anomaly below T_N be attributed to a magnetic phase transition of the coexisting tetragonal phase in samples used by Zhu *et al.*[23] The answer is no, since the Néel temperature for the tetragonal phase lies well below room temperature,[21,23] whereas the broad anomaly in $M(T)$ below T_N occurs well above room temperature. It is known that the stress-induced coexisting tetragonal phase disappears on annealing above 973 K, leaving behind pure monoclinic compositions.[24] The results presented here are on well-annealed samples containing monoclinic phase only. Thus, the anomaly observed in $M(T)$ below the Néel temperature in BF-xPT with x = 0.25 and 0.27 by us or Zhu *et al.* cannot be attributed to the presence of any coexisting orthorhombic (which in any case does not exist in the BF-xPT system[16]) or the tetragonal phase whose T_N lies well below room temperature.[21]

C. Absence of structural phase transition and magnetoelastic coupling at T_{OPT}

To verify if the broad anomaly in $M(T)$ at T_{OPT} is due to a structural phase transition, we carried out XRD studies of the crystal structure as a function of temperature. The powder diffraction profiles of 110 and 111 pseudocubic peaks of BF-xPT for $x = 0.27$ at various temperatures are depicted in Fig. 2. The first two patterns at $T = 300$ and 323 K correspond to the phase below the $T_{OPT} \sim 367$ K. The diffraction patterns at 398, 423, and 448 K correspond to the structure in the temperature range $T_{OPT} < T < T_N = 473$ K, while patterns above 473 K represent the structure of the paramagnetic phase ($T > T_N$). It is evident from the evolution of the diffraction profiles as a function of temperature that except for a gradual shift in the peak positions toward the lower 2θ side with increasing temperature due to thermal expansion, the basic nature of the profiles does not change. This was confirmed by Rietveld refinements also that show the presence of the monoclinic phase in the Cc space group from room

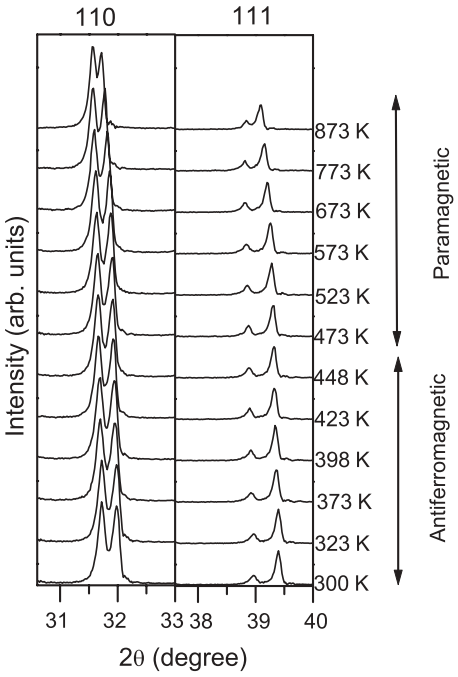

FIG. 2. Evolution of the 110 and 111 pseudocubic reflections of BF-0.27PT with temperature showing absence of structural phase transition at T_N and T_{OPT}.

temperature to well above T_N. This confirmed the absence of any structural phase transition either across T_N or T_{OPT}.

The variation of unit cell volume as obtained by Rietveld refinement is depicted in Fig. 3. The data for $T \geqslant 365$ K in this figure were published earlier in Ref. 21, and we have added additional data points in Fig. 3 to cover the temperatures below T_{OPT}. It is evident from this figure that the AFM transition at $T \sim 473$ K is accompanied by a small change in the unit cell volume, as already discussed in Ref. 21, but there is no such anomaly at the $T_{OPT} \sim 367$ K. These observations reveal the presence of magnetoelastic coupling at T_N but not at T_{OPT}. We, therefore, conclude that the anomaly in $M(T)$ at T_{OPT} is not

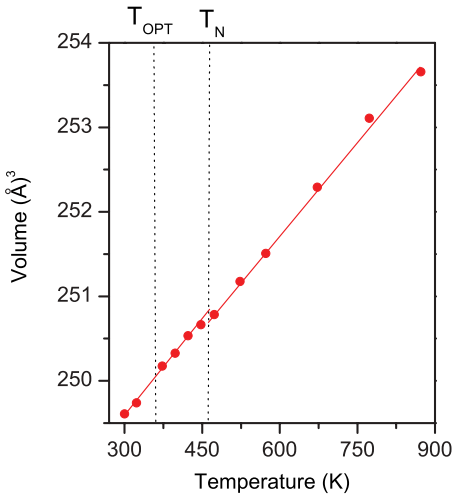

FIG. 3. (Color online) The variation of unit cell volume of BF-0.25PT with temperature showing signature of magnetoelastic coupling at T_N but absence of any anomaly at T_{OPT}.

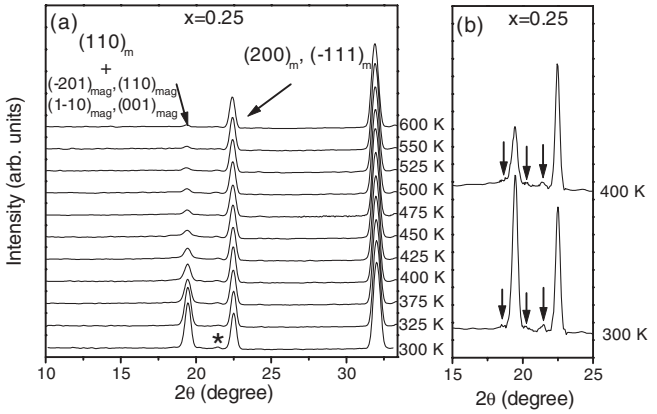

FIG. 4. (a) Temperature-dependent neutron powder diffraction profiles of BF-0.25PT in the 2θ range from 10 to 32.5°. The reflections $(200)_m$, $(-111)_m$, and $(110)_m$ are from monoclinic nuclear cell. Expected positions of modulation peaks ($\boldsymbol{k} = 0,0,\delta$ with $\delta \sim 0.1$) are marked with arrows (b).

due to a structural phase transition and that this transition is purely of magnetic origin with little magnetoelastic coupling.

D. Evidence for the presence of two different magnetic structures below the Néel transition

In order to understand the origin of the second anomaly in $M(T)$ below T_N, we decided to investigate the magnetic structure as a function of temperature using neutron powder diffraction data. Figure 4(a) depicts the temperature evolution of the neutron powder diffraction profiles for $x = 0.25$ in the 2θ range from 10 to 32.5°. The first peak at $2\theta \sim 19.5°$ is due to the antiferromagnetic ordering, and its intensity decreases on increasing the temperature toward $T_N \sim 483$ K. There is a small residual intensity even above T_N due to short-range antiferromagnetic correlations. The existence of small residual intensity above T_N, determined from $M(T)$ measurements, is well known in pure $BiFeO_3$ and its solid solutions.[25]

The main magnetic reflections of BF-0.25PT can be indexed with a propagation vector $\boldsymbol{k} = 0,0,0$ indicating that the translation symmetry is not lost in the magnetically ordered phase below T_N. The magnetic representation of the Fe sublattice (4*a* Wyckoff site) can be decomposed into two IRs, each with three basis vectors, i.e., $\Gamma^{4a} = 3[\Gamma_1{}^{000} + \Gamma_2{}^{000}]$, leading to two possible configurations of the magnetic moments in the monoclinic phase (see Supplementary Material of Ref. 21 for the character table and basis vectors). As has been shown elsewhere,[21] the magnetic structure of BF-xPT at room temperature for the monoclinic composition corresponds to a noncollinear antiferromagnetic ordering that can be expressed as ($\boldsymbol{G_{xz}}$, $\boldsymbol{F_y}$) in Bertaut's notation.[9] It corresponds to the $\Gamma_1{}^{000}$ IR of the Brillouin zone center (i.e., with a propagation vector, $\boldsymbol{k} = 0,0,0$ in Ref. 21). This structure explains well all the observed diffraction peaks at room temperature and higher temperatures below the broad magnetic anomaly temperature, i.e., T_{OPT}. However, above the broad magnetic anomaly temperature (T_{OPT}), this model is not adequate. The results of Rietveld refinements with Γ_1 representation (see the Supplementary Material of Ref. 21 for more details about this representation) carried out below T_{OPT} and between T_{OPT} and T_N are compared in Figs. 5(a) and 5(c). It is evident from these figures that while the Γ_1 representation gives a nice fit to the observed neutron diffraction pattern, including the magnetic peaks at 300 K (i.e., below T_{OPT}), it fails to model the magnetic superlattice peak at 425 K [see inset of Fig 5(c)], which lies in the temperature range $T_{OPT} < T < T_N$.

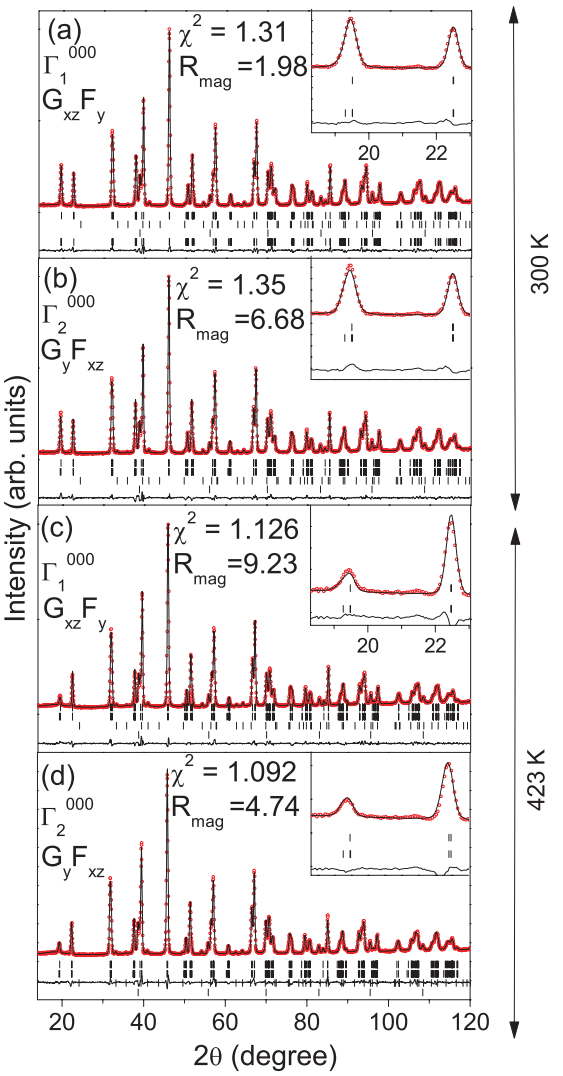

FIG. 5. (Color online) Observed (dotted), calculated (continuous line), and difference profiles (bottom line) obtained from Rietveld refinement of BF-0.25PT in the monoclinic *Cc* space group with two possible magnetic structures corresponding to (a) Γ_1 ($\boldsymbol{k} = 0,0,0$ and (b) Γ_2 ($\boldsymbol{k} = 0,0,0$) at $T = 300$ K and (c) Γ_1 ($\boldsymbol{k} = 0,0,0$) and (d) Γ_2 ($\boldsymbol{k}$ 0,0,0) at $T = 423$ K.

As the translational symmetry remains the same below and above the two anomalies in $M(T)$, the second model corresponding to the Γ_2 representation of the zone center was considered as the next possibility. The results of Rietveld refinements are shown in Figs. 5(b) and 5(d) for $T = 300$ and 425 K, respectively. At 300 K, a slight mismatch occurs between the observed and calculated profiles for the magnetic reflection, as can be seen from the inset of Fig. 5(b). The R_{mag} for the Γ_2 representation is also much higher ($R_{mag} = 6.68$) than that for Γ_1 ($R_{mag} = 1.98$) at 300 K, as already discussed in the previous section. The Γ_2 representation, on

TABLE I. The symmetry-adapted strain and the corresponding reduced space group symmetry.

IR	Symmetry-adapted strain	Reduced space group
Γ_1	$e_{xx}, e_{yy}, e_{zz}, e_{xz}$	Cc
Γ_2	e_{xy}, e_{yz}	$P1$

the other hand, explains very well the observed diffraction pattern, including the main magnetic peak at 425 K and gives smaller value of R_{mag} as compared to that for Γ_1: $R_{\mathrm{mag}} = 9.23$ and 4.72 for Γ_1 and Γ_2, respectively. In this model (i.e., the Γ_2 representation), the ferromagnetic component of the magnetic moment can rotate in the xz plane ($\boldsymbol{F}_{xz}$), but the antiferromagnetic component, $\boldsymbol{G}_y$, is confined to the y axis. This has similarity with rare-earth orthoferrites, in which the ferromagnetic component ($\boldsymbol{F}_{xz}$) of iron moments orients continuously from along c axis toward the a axis in the temperature range T_1 to T_2 as a result of spin-reorientation phase transition.[2–5] Accordingly, a possible explanation can be sought for the observed anomaly in the magnetization data at $T \sim 360$ and 373 K for $x = 0.25$ and 0.27, respectively, as being due to a spin-reorientation phase transition of iron magnetic sublattice and hence a change in the magnetic structure from the Γ_1 to Γ_2 representation. If this is true, the sequence of magnetic transitions with increasing temperature should be as follows:

$$\Gamma_1\,(\boldsymbol{G}_{xz}, \boldsymbol{F}_y) \rightarrow \Gamma_2\,(\boldsymbol{G}_y, \boldsymbol{F}_{xz}) \rightarrow \text{Paramagnetic}.$$

However, the above scheme of transitions is not consistent with the absence of change in crystal symmetry across T_{OPT}, since the Γ_1 representation is a symmetry preserving IR but Γ_2 is not. So, if the magnetic transition follows the above-mentioned sequence, involving the Γ_2 representation, then there should be a structural change with the onset of magnetic ordering from paramagnetic phase to antiferromagnetic phase at T_N. The symmetry-adapted strain and the corresponding space group to which the symmetry of the parent paramagnetic phase, Cc, will get reduced as a result of magnetoelastic coupling is listed in Table I. While the paramagnetic to antiferromagnetic transitions at T_N in the monoclinic compositions of BF-xPT is associated with a strong magnetoelastic effect, there is no change in the space group of the nuclear structure, which remains the same (Cc) both above T_N and below T_N, as can be seen from Fig. 2 also. Therefore, the Γ_2 representation, even though it gives good fit to the entire diffraction pattern, including the main magnetic peak between T_{OPT} and T_N, can also be ruled out.

In order to determine the magnetic structure at $T_{\mathrm{OPT}} < T < T_N$, other possible propagation vectors than $\boldsymbol{k} = 0,0,0$ have to be considered such that they retain the translational symmetry of the nuclear structure and the associated symmetry-adapted strain does not lower the space group symmetry of the nuclear structure. Table SI in Supplementary Material[26] lists high-symmetry points, lines, a plane, and a general point in the reciprocal lattice of the monoclinic Cc space group. The possible values of the propagation vector that can retain the translational symmetry of the nuclear cell are listed in Supplementary Material in Table SII.[26] Since the propagation vector $\boldsymbol{k} = 0,0,0$ cannot account for the magnetic structure

TABLE II. Character table and basis vector (magnetic) of space group Cc at $\boldsymbol{k} = 0,0,1$.

IR	Symmetry elements (Kovalev)			
	$\{1\|0,0,0\}$	$\{\sigma\|0.5,0,0\}$		
Γ_1^{001}	1	1		
Γ_2^{001}	1	-1		
IR	Basis vector		$4a$ site	
			(x,y,z)	$(x,-y,z+1/2)$
Γ_1^{001}	$\tau_{1,1}$	Re	(1 0 0)	($-$1 0 0)
		Im		
	$\tau_{1,2}$	Re	(0 1 0)	(0 1 0)
		Im		
	$\tau_{1,3}$	Re	(0 0 1)	(0 0 $-$1)
		Im		
Γ_2^{001}	$\tau_{2,1}$	Re	(1 0 0)	(1 0 0)
		Im		
	$\tau_{2,2}$	Re	(0 1 0)	(0 $-$1 0)
		Im		
	$\tau_{2,3}$	Re	(0 0 1)	(0 0 1)
		Im		

above T_{OPT}, in the next step, magnetic models corresponding to other propagation vectors lying along c^* axis in the Brillouin zone, commonly called as LD line (LD stands for the Greek letter Λ, see also Tables SI and SII in the Supplementary Material[26]) were considered. It was verified that only $\boldsymbol{k} = 0,0,1$ propagation vector can account for the entire diffraction pattern, including the main magnetic peak. There are two IRs (Γ_1^{001} and Γ_2^{001}) for the propagation vector $\boldsymbol{k} = 0,0,1$. The character table and the basis vectors of the two IRs are shown in Table II. Figures 6(a) and 6(b) depict the calculated, observed, and difference profiles obtained by Rietveld refinement of the magnetic structures considering the two IRs, i.e., Γ_1^{001} and Γ_2^{001}, respectively. The magnetic model with Γ_2^{001} gives excellent fit for the observed diffraction profile, including the main magnetic peak, as can be seen from the inset to Fig. 6(b). The second IR (Γ_1^{001}) misses the magnetic peak considerably as shown in the inset to Fig. 6(a). The magnetic structure of BF-0.25PT in the temperature range $T_{\mathrm{OPT}} < T < T_N$ is modeled with the Γ_2^{001} representation that corresponds to ($\boldsymbol{G}_y$,$\boldsymbol{F}_{xz}$) in Bertaut's notation. Table III lists the refined structural parameters, thermal parameters, ordered magnetic moments, and the agreement factors.

For the IR Γ_2^{001} with the propagation vector $\boldsymbol{k} = 0,0,1$, the coupling between the primary-order parameter ($\boldsymbol{F}_{xz}$ and $\boldsymbol{G}_y$) and the secondary-order parameter (the strain field) can be built by looking at the decomposition onto IRs of the symmetrized square of Γ_2^{001} (see Table IV).[27] The decomposition in terms of IRs at the zone center is $[\Gamma_2^{001}]^2 = \Gamma_1$. Thus, the strain field associated with Γ_2^{001} corresponds to the symmetry-preserving IR, Γ_1, at the zone center, and so the magnetoelastic coupling at T_N will not lower the space group symmetry for the Γ_2^{001} at $\boldsymbol{k} = 0,0,1$ representation in agreement with the absence of any structural change accompanying the transition at T_N.

It is important to mention that the true magnetic structure of the monoclinic phase of BF-xPT may have a long-range

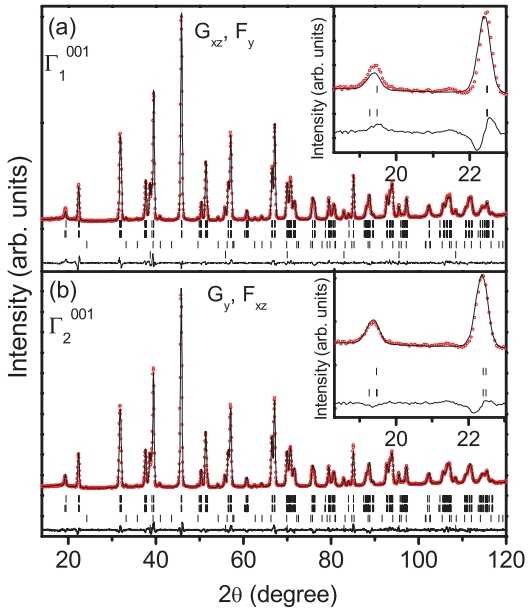

FIG. 6. (Color online) Observed (dotted), calculated (continuous line), and difference profiles (bottom line) obtained from Rietveld refinement of BF-0.25PT in the monoclinic Cc space group with two possible magnetic structures corresponding to (a) Γ_1 ($\boldsymbol{k}$ = 0,0,1), (b) Γ_2 ($\boldsymbol{k}$ = 0,0,1) at T = 423 K.

modulation of magnetic moments, superimposed on the G-type noncollinear antiferromagnetic structure similar to that of the parent compound $BiFeO_3$ (BF[11,28]) and Mn-substituted BF.[29] It is interesting to note that there is a small hump at $2\theta \sim 21.5^\circ$ (see Fig. 4), which shows a temperature dependence similar to the main magnetic peak. We have been able to index this weak peak with a propagation vector $\mathbf{k} = 0,0,\delta$, with $\delta = 0.096 + / - 0.0004$. Such a propagation vector predicts two more satellite peaks near the main magnetic peak at $2\theta \sim 18.9^\circ$ and 20.05° in excellent agreement with the experimental observations depicted in Fig. 4(b) on a magnified scale. Since these magnetic satellite peaks have very low intensity, it was not possible to see the effect of reorientation transition on the magnetic modulation structure. Further, the present resolution of the neutron data is not adequate to determine whether this modulation is a commensurate or incommensurate type.

TABLE IV. Symmetrized square of IRs.

$\boldsymbol{k}$ vector level	IR	Symmetrized square $(\mathrm{IR})^2$
LD	Γ_1^{001}	$[\Gamma_1^{001}]^2 = \Gamma_1$
	Γ_2^{001}	$[\Gamma_2^{001}]^2 = \Gamma_1$

It may, however, be noted that the anomaly in $M(T)$ around the reorientational transition temperature T_{OPT} is stronger than the anomaly observed around the antiferromagnetic transition temperature (T_N), and it, therefore, indicates a strong rearrangement of the magnetic moments across the reorientation transition. Small changes in the long-range modulation (i.e., change in the q value) may not lead to such a drastic change in $M(T)$, although higher resolution diffraction data are required to investigate this aspect of the spin-reorientation transition in BF-xPT.

Thus, to summarize the results of this section, BF-xPT for $x = 0.25$ and 0.27 undergoes the following magnetic transitions:

$$\Gamma_1^{000}(\boldsymbol{G_{xz}}, \boldsymbol{F_y}) \rightarrow \Gamma_2^{001}(\boldsymbol{G_y}, \boldsymbol{F_{xz}}) \rightarrow \text{Paramagnetic}.$$

It is evident from this sequence of phase transition that the $\boldsymbol{F_{xz}}$ component that lies in the xz plane jumps by 90° and becomes $\boldsymbol{F_y}$ below T_{OPT}. The refined patterns in Figs. 5 and 6 correspond to the nuclear and magnetic contribution of BF-0.25PT as well as that of the sample holder (Nb) and trace amount of Fe_2O_3 (<2%). The refined structural parameters and the ordered magnetic moments of Fe for models corresponding to Γ_1^{000} at T = 300 K and that corresponding to Γ_2^{001} at T = 423 K are given in Table III. The sequence of change in magnetic structure across T_{OPT} in terms of $\boldsymbol{F}$ and $\boldsymbol{G}$ vectors is shown in Fig. 7.

TABLE III. Reitveld refined position coordinates, thermal parameters, and lattice parameters of BF-0.25PT in the monoclinic space group Cc at temperatures 300 and 425 K.

Composition of BF-0.25PT	Atom	Fractional x,	Coordinates y,	z	Thermal parameters (Å^2)	Lattice parameters (Å)	Statistical parameter
T = 300 K							
	Bi/Pb:	0.0,	0.25,	0.0	1.46(3)	$a = 9.7832(1)$	$R_p = 3.22$, $R_{wp} = 4.12$
	Fe/Ti:	0.2751(8),	0.253(1),	0.731(1)	0.43(3)	$b = 5.5872(9)$	$R_{exp} = 3.55$, $\chi^2 = 1.35$
	O1:	0.046(5),	0.301(1),	0.4599(9)	1.1(1)	$c = 5.6312(2)$	$R_{mag} = 1.98$
	O2:	0.327(4),	0.482(7),	0.0338(7)	0.68(9)	$\alpha = \gamma = 90$	
	O3:	0.284(7),	−0.025(1),	−0.0491(8)	1.0(1)	$\beta = 125.78(1)$	
$\mu_B = 3.46$ (at T = 300 K with Γ_1^{000} model)							
T = 423 K							
	Bi/Pb:	0.0,	0.25,	0.0	1.76(2)	$a = 9.8071(1)$	$R_p = 2.92$, $R_{wp} = 3.86$
	Fe/Ti:	0.2740(8)	0.250(1),	0.731(2)	0.76(4)	$b = 5.5899(6)$	$R_{exp} = 3.41$, $\chi^2 = 1.096$
	O1:	0.0359(5),	0.282(1),	0.4562(9)	1.30(7)	$c = 5.6358(4)$	$R_{mag} = 4.71$
	O2:	0.321(5),	0.480(4),	0.0246(7)	0.99(7)	$\alpha = \gamma = 90$	
	O3:	0.270(5),	−0.041(1),	−0.0536(8)	1.14(6)	$\beta = 125.70(2)$	
$\mu_B = 1.74$ (at T = 425 K with Γ_2^{001} model)							

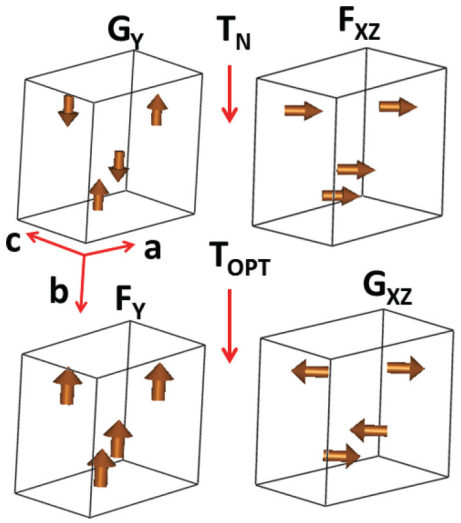

FIG. 7. (Color online) Schematic depiction of the $\boldsymbol{F}$ and $\boldsymbol{G}$ components of the two magnetic structures of BF-0.25PT above and below T_{OPT}.

E. Comparison with theoretical predictions for spin-reorientation transition

Since the preferred direction of the magnetic moment is determined by the magnetic anisotropy energy, the reorientation of magnetic spins below the T_{OPT} transition is governed by the temperature variation of the anisotropy energy acting upon the spin system. To describe the nature of spin-reorientation transition in iron-based insulating antiferromagnets, Levinson *et al.*[30] have considered the following spin Hamiltonian

$$H = H_0 + H_a, \tag{1}$$

where $H_0 = -\sum_{i\neq j} J_{ij}\vec{S}_i.\vec{S}_j$ is the isotropic Heisenberg Hamiltonian and

$$H_a = \sum_i \kappa_2\left(S_i^z\right)^2 + \sum_i \kappa_4\left(S_i^z\right)^4 + \sum_{i\neq j} \kappa_{1,ij} S_i^z S_j^z \tag{2}$$

represents the second- and fourth-order spin anisotropy and is assumed to depend only on S_z, making the easy-axis reorientation only in a single plane, i.e., the xz plane. If the mean magnetic moment $\langle S\rangle$ at temperature T points along $\boldsymbol{n}$, where $\boldsymbol{n}$ is a unit vector making an angle θ with the z axis, the average value of the anisotropic part of the free energy given by Eq. (3) takes the usual form considered in the phenomenological theory of spin-reorientation transition[31]

$$\langle H_a\rangle = A_0(T) + A_2(T)\sin^2\theta + A_4(\mathrm{T})\sin^4\theta, \tag{3}$$

where $A_0(T)$, $A_2(T)$, and $A_4(T)$ are, in general, temperature dependent.

This form of free energy predicts first-order and second-order reorientation transitions corresponding to $A_4 < 0$ and $A_4 > 0$, respectively.[31] In the second-order reorientation transition, the magnetization vector rotates continuously on the easy plane from $\theta = 0$ ($\boldsymbol{F}_x$) to $\theta = 90$ ($\boldsymbol{F}_z$) through intermediate values of $\theta \in [0,90]$. The spin-reorientation transition in most orthoferrites corresponds to such a second-order transition. The first-order reorientation transition corresponds to the spin flop, where the magnetization vector jumps from $\theta = 0$ to $\theta = 90$ at T_{OPT} as in the Morin transition.[1] In

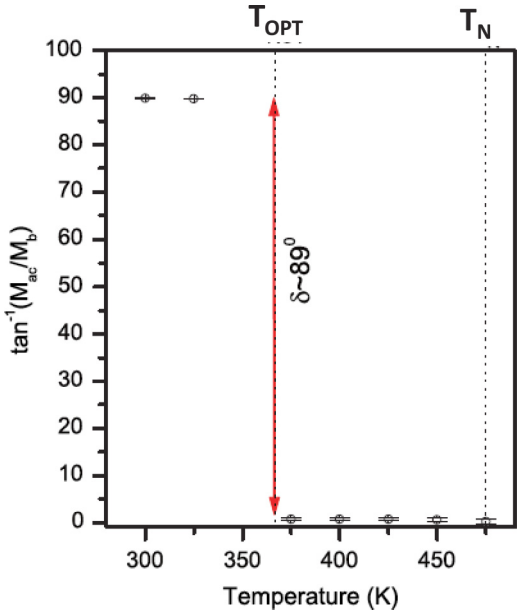

FIG. 8. (Color online) Variation of angle $\tan^{-1}(M_{\mathrm{ac}}/M_{\mathrm{b}})$ with temperature.

case of BF-xPT, the noncollinear magnetic structure at room temperature has the antiferromagnetic component in the ac plane ($\boldsymbol{G}_{xz}$ with magnitude $M_{ac} = 3.465\ \mu_{\mathrm{B}}$ per Fe^{3+} site at 300 K) and a very weak ferromagnetic component along b axis ($\boldsymbol{F}_y$ with magnetiude $M_b = 0.018\ \mu_{\mathrm{B}}$ per Fe^{3+} site). Because of the very small value of the out of ac plane component of M, the magnetization vector (per Fe^{3+} site) is essentially contained in the ac plane. Similarly, above the reorientation transition temperature (T_{OPT}), the ferromagnetic component of the magnetization in the ac plane is very weak ($M_b = 1.741\mu_{\mathrm{B}}$, $M_{ac} = 0.02\mu_{\mathrm{B}}$ per Fe^{3+} site), and as a result, the magnetization vector is essentially along the b axis. We have attempted to calculate the change in the angle θ of the net magnetization vector with respect to the b axis from the refined values of M_b and M_{ac} as a function of temperature but this change, if any, is within the standard deviations. Thus, θ is nearly 90° below T_{OPT} and becomes nearly zero just above T_{OPT} as shown in Fig. 8. Within the limits of the resolution of the present refinement, the spin-reorientation transition is therefore of first-order type.

IV. SUMMARY

To summarize, we have presented unambiguous evidence for the existence of a spin-reorientation transition in the monoclinic compositions of BF-xPT below the antiferromagnetic transition temperature (T_N) using magnetization and neutron scattering measurements. The paramagnetic phase of the monoclinic compositions of BF-xPT undergoes two transitions: first a Néel transition to a long-range magnetically ordered phase ($\boldsymbol{G}_y$, $\boldsymbol{F}_{xz}$) at T_N and then a spin-reorientation transition to another long-range magnetically ordered phase ($\boldsymbol{G}_{xz}$, $\boldsymbol{F}_y$) at T_{OPT} wherein the ferromagnetic component of the noncollinear magnetic structure undergoes a spin flop. The spin-reorientation transition at T_{OPT} does not involve change of crystal symmetry and the space group. Further, there is no signature of magnetoelastic coupling in the temperature variation of the unit cell volume at T_{OPT}. Our results thus

suggest that the spin-reorientation transition in monoclinic compositions of BF-xPT is of purely magnetic origin.

ACKNOWLEDGMENTS

D.P. acknowledges support from the Department of Science and Technology, Government of India, and the Japan Society for the Promotion of Science, Japan, under its Indo-Japan collaboration program. S.B. acknowledges the award of Senior Research Fellowship of Council of Scientific and Industrial Research, India. D.P. and S.B. acknowledge the assistance of R. K. Kotnala and V. Pandey of the National Physical Laboratory, New Delhi for magnetization measurements. The authors are grateful to the Forschungsneutronenquelle Heinz Maier-Leibnitz for providing support during the neutron scattering experiments. We thank Anar Singh for collecting the neutron diffraction data. We also thank Y. Kuriowa and C. Moriyoshi for reading the manuscript. D. Pandey acknowledges financial support from DST of India through J.C. Bose National Fellowship grant.

*dp.mst1979@gmail.com

[1]R. Nathas, S. J. Pickart, H. A. Alperin, and P. J. Brown, Phys. Rev. **136**, A1641 (1964); D. Schroeer and R. C. Nininger, Jr., Phys. Rev. Lett. **19**, 632 (1967); D. C. Herbert, *ibid.* **22**, 1184 (1969); P. Kuiper, B. G. Searle, P. Rudolf, L. H. Tjeng, and C. T. Chen, *ibid.* **70**, 1549 (1993).

[2]W. P. Wolf and R. L. White, J. Appl. Phys. **40**, 1061 (1969); V. D. Buchel'nikov, N. K. Dan'shin, L. T. Tsymbal, and V. G. Shavrov, Phys. Usp. **39**, 547 (1996).

[3]Y. B. Bazaliy, L. T. Tsymbal, G. N. Kakazei, A. I. Izotov, and P. E. Wigen, Phys. Rev. B **69**, 104429 (2004).

[4]L. T. Tsymbal, V. I. Kamenev, Ya. B. Bazaliy, D. A. Khara, and P. E. Wigen, Phys. Rev. B **72**, 052413 (2005).

[5]K. P. Belov, R. A. Volkov, B. P. Goranskii, A. M. Kadomtseva, and V. V. Uskov, Sov. Phys. Solid State **11**, 935 (1969); H. Pinto, G. Shachar, H. Shaked, and S. Shtrikman, Phys. Rev. Lett. **3**, 3961 (1971); V. D. Doroshev, A. S. Kharnachev, N. M. Kovtun, E. E. Soloviev, A. Ya. Chervonenkis, and A. A. Shemyakov, Phys. Status Solidi B **51**, K31 (1972); N. M. Kovtun, A. S. Karnachev, E. E. Soloviev, A. Ya. Chevonenkis, and A. A. Shemyakov, Sov. Phys. Solid State **14**, 1856 (1973); S. M. Shapiro, J. D. Axe, and J. P. Remeika, Phys. Rev. B **10**, 2014 (1974).

[6]N. P. Duong, T. Satoh, and M. Fiebig, Phys. Rev. Lett. **93**, 117402 (2004); T. Kampfrath, A. Sell, G. Klatt, A. Pashkin, S. Mahrlein, T. Dekorsy, M. Wolf, M. Fiebig, A. Leitenstorfer, and R. Huber, Nat. Photonics **5**, 31 (2011).

[7]C. Frandsen and S. Morup, Phys. Rev. Lett. **94**, 027202 (2005).

[8]A. V. Kimel, A. Kirilyuk, A. Tsvetkov, R. V. Pisarev, and Th. Rasing, Nature (London) **429**, 850 (2004); A. V. Kimel, B. A. Ivanov, R. V. Pisarev, P. A. Usachev, A. Kirilyuk, and Th. Rasing, Nat. Phys. **5**, 727 (2009).

[9]E. F. Bertaut, Acta Crystallogr. Sec. A **24**, 217 (1968).

[10]A. M. Glazer, Acta Crystallogr. Sec. B **28**, 3384 (1972); Acta Crystallogr. Sec. A **31**, 756 (1975).

[11]I. Sosnowska, T. Peterlin-Neumaier, and E. Steichele, J. Phys. C **15**, 4835 (1982).

[12]R. Haumont, I. A. Kornev, S. Lisenkov, L. Bellaiche, J. Kreisel, and B. Dkhil, Phys. Rev. B **78**, 134108 (2008); M. Polomska, A. W. Kavzmare, and Z. Pajak, Phys. Status Solidi **23**, 567 (1974).

[13]M. K. Singh, W. Prellier, M. P. Singh, R. S. Katiyar, and J. F. Scott, Phys. Rev. B **77**, 144403 (2008).

[14]M. Ramazanoglu, W. Ratcliff, Y. J. Choi, S. Lee, S.-W. Cheong, and V. Kiryukhin, Phys. Rev. B **83**, 174434 (2011); J. Lu, M. Schmidt, P. Lunkenheimer, A. Pimenov, A. A. Mukhin, V. D. Travkin, and A. Loidl, J. Phys.: Conf. Ser. **200**, 012106 (2010).

[15]S. Bhattacharjee, V. Pandey, R. K. Kotnala, and D. Pandey, Appl. Phys. Lett. **94**, 012906 (2009).

[16]S. Bhattacharjee and D. Pandey, J. Appl. Phys. **107**, 124112 (2010).

[17]S. Bhattacharjee, S. Tripathi, and D. Pandey, Appl. Phys. Lett. **91**, 042903 (2007).

[18]M. Hoelzel, A. Senyshyn, N. Juenke, H. Boysen, W. Schmahl, and H. Fuess, Nucl. Instrum. Methods Phys. Res. Sect. A **667**, 32 (2012).

[19]J. Rodriguez-Carvajal Laboratory, FULLPROF, a Rietveld and pattern matching analysis program, Laboratoire Leon Brillouin-CEA-CNRS, France. http://www.ill.eu/sites/fullprof/.

[20]R. J. Zeches, M. D. Rossell, J. X. Zhang, A. J. Hatt, Q. Hatt, Q. He, C.-H. Yang, A. Kumar, C. H. Wang, A. Melville, C. Adamo, G. Sheng, Y.-H. Chu, J. F. Ihlefeld, R. Erni, C. Ederer, V. Gopalan, L. Q. Chen, D. G. Schlom, N. A. Spaldin, L. W. Martin, and R. Ramesh, Science **326**, 977 (2009); I. C. Infante, S. Lisenkov, B. Dupe, M. Bibes, S. Fusil, E. Jacquet, G. Geneste, S. Petit, A. Courtial, J. Juraszek, L. Bellaiche, A. Barthelemy, and B. Dkhil, Phys. Rev. Lett. **105**, 057601 (2010).

[21]S. Bhattacharjee, A. Senyshyn, P. S. R. Krishna, H. Fuess, and D. Pandey, Appl. Phys. Lett. **94**, 262506 (2010).

[22]W. Kaczmarek, Z. Pajak, and M. Polomska, Solid State Commun. **17**, 807 (1975).

[23]W. M. Zhu, H. Y. Guo, and Z. G. Ye, Phys. Rev. B **78**, 014401 (2008).

[24]S. Bhattacharjee and D. Pandey, J. Appl. Phys. **110**, 084105 (2011).

[25]C. M. Yagnik, R. Gerson, and W. J. James, J. Appl. Phys. **42**, 395 (1971); A. Singh, A. Senyshyn, H. Fuess, T. Chatterji, and D. Pandey, Phys. Rev. B **83**, 054406 (2011).

[26]See Supplemental Material at http://link.aps.org/supplemental/10.1103/PhysRevB.87.054417 for high symmetry points, lines, a plane, and a general point in the reciprocal lattice of the monoclinic Cc space group (Table S1) and the possible values of the propagation vector that can retain the translational symmetry of the nuclear cell in Cc space group symmetry (Table S2). The tables are obtained using software package ISOTROPY, http://stokes.byu.edu/iso/isotropy.html. For convention of used symbols refer to "ISOTROPY Tutorial 2007" page 9 at the site http://stokes.byu.edu/iso/isotropy.html.

[27]Programs DIRPRO and CORREL, Bilbao crystallographic server. http://www.cryst.ehu.es/.

[28]R. Przeniosło, A. Palewicz, M. Regulski, I. Sosnowska, R. M. Ibberson, and K. S. Knight, J. Phys.: Condens. Matter **18**, 2069 (2006).

[29]I. Sosnowska, W. Schäfer, W. Kockelmann, K. H. Andersen, and I. O. Troyanchuk. Appl. Phys. A **74**, S1040 (2002).

[30]L. M. Levinson, M. Luban, and S. Shtrikman, Phys. Rev. **187**, 715 (1969).

[31]H. Horner and C. M. Varma, Phys. Rev. Lett. **20**, 845 (1968).